Predicting density wave amplification of settling slurries using a 1D Driftux model

de Hoog, E.; van Wijk, J. M.; Talmon, A. M.; van Rhee, C.

DOI
10.1016/j.powtec.2022.117252

Publication date
2022

Document Version
Final published version

Published in
Powder Technology

Powder Technology 400 (2022) 117252

Contents lists available at ScienceDirect

Powder Technology

journal homepage: www.elsevier.com/locate/powtec

Predicting density wave amplification of settling slurries using a 1D Driftux model

E. de Hoog [a,*], J.M. van Wijk [b], A.M. Talmon [c], C. van Rhee [c]

[a] R&D Engineer, Royal IHC, Smitweg 6, Kinderdijk 2961 AW, the Netherlands
[b] Manager advisory services, IHC IQIP, Molendijk 94, Sliedrecht 3361 EW, the Netherlands
[c] Dept. Dredging, Trenching and Deep Sea Mining Technology, Delft University of Technology, Mekelweg 2, Delft 2628 CD, the Netherlands

ARTICLE INFO

Article history:
Received 28 September 2021
Received in revised form 9 February 2022
Accepted 27 February 2022
Available online 3 March 2022

Keywords:
Hydraulic transport
Hydraulic transients
Flow assurance
1D Driftflux model
Dredging
Deep sea mining

ABSTRACT

Density wave amplification in hydraulic transport pipelines forms a high risk to operational continuity, as density waves can lead to system blockages or centrifugal pump drive failures. Recent experimental research, in pipelines which contain long vertical sections, has shown that density waves can amplify at velocities far exceeding the deposit limit velocity, previously thought to be a limiting condition for amplification. The typical design methodology of hydraulic transport pipelines is based on a steady-state philosophy, which assumes that the mixture velocity and sediment concentration are constant in time and space. However, these variations can lead to the amplification of density waves. This article discusses the cause of a new type of density wave amplification mechanism, which is related to slurry dynamics in a pipeline containing vertical sections. This research also presents a 1D Driftflux CFD model which models the aforementioned slurry dynamics and can predict density wave amplification.

1. Introduction

Density waves in hydraulic transport pipeline are very common, caused by fluctuating solids influx. These fluctuations are caused by the nature of the excavation process typically feeding these pipelines, and by the dredge operators actions. In the 1980's it was discovered that density waves could amplify while flowing through the pipeline, when the bulk velocity was too close to the deposition limit velocity, defined as the threshold velocity at which particles settle out of suspension and form a deposit in the pipeline. Research by [1–4] laid the foundation for understanding density wave amplification for horizontal pipelines, caused by an inverse relationship between sedimentation and erosion of sand deposits in a pipeline when the pipeline operates close to the deposit limit velocity. This is referred to the "erosion and sedimentation imbalance", and as a result high concentration zones of a slurry erode deposits and low concentration parts form deposits [3,5]. As such, a spatial redistribution occurs with sediment redistributing from low density parts to high density parts of the flow. Density wave amplification in horizontal pipelines can be avoided by remaining well above the deposit limit velocity, preferably with a safety margin to compensate for inaccuracies in deposit limit velocity predictive models and to account for velocity variations due to pipeline-pump dynamics [5].

Recent experimental research into vertical hydraulic transport technology for deep sea mining [6] showed density wave amplification occurring far above the deposition limit velocity. These experiments, referred to as the "Freiberg experiments," were conducted in a closed loop pipe circuit, containing long vertical sections and some horizontal pipes to facilitate a centrifugal pump and soil injection and separation equipment (more details can be found in chapter 3.1). A combined vertical and horizontal loop is designed based upon the deposit limit velocity of the horizontal pipes, as the minimum design velocity of vertical pipes is typically lower (which is typically two or thee times the terminal settling velocity of the largest particles [7]). The Freiberg experiments showed density wave amplification in all tests at mixture velocities significantly above the deposit limit velocity of the horizontal pipes (sometimes double). The amplification rate seemed to depend on the particle size, the average volumetric concentration and the mixture velocity relative to the deposit limit velocity (more details in chapter 3.1). The origins of the mechanism behind amplification was explored by [5] and was thought to be caused by a different and new mechanism as opposed to the erosion and sedimentation imbalance. The authors of [5] hypothesized that amplification can be caused by a reduction of the particle velocity when particles flow from vertical to horizontal pipes resulting in an increase in concentration, referred to as "transient accumulation." This article continues with work of [5] and explains transient accumulation and presents the Freiberg vertical transport experiments which were subject to this new type of density wave amplification.

* Corresponding author.
E-mail address: e.dehoog@royalihc.com (E. de Hoog).

https://doi.org/10.1016/j.powtec.2022.117252
0032-5910/

List of symbols

ε	Diffusion coefficient $[m^2/s]$
ρ_f	Water density $[kg/m^3]$
ρ_m	Mixture density $[kg/m^3]$
ρ_s	Solids density $[kg/m^3]$
τ_s	Shear stress caused by the solids $[Pa]$
τ_f	Shear stress caused by the fluid $[Pa]$
τ_m	Shear stress caused by the mixture $[Pa]$
τ_{ml}	Shear stress caused by minor losses $[Pa]$
ω	Pipe inclination angle $[rad]$
μ_{sf}	Sliding friction factor between a sliding granular bed and the pipe wall $[-]$
ν_f	Kinematic viscosity of the fluid $[m^2/s]$
A	Cross sectional area $[m^2]$
c	Volumetric concentration of solids $[-]$
c_{max}	Maximum concentration $[-]$
C_d	Drag coefficient $[-]$
c_{vd}	Volumetric delivered concentration of solids $[-]$
d	Particle diameter $[m]$
d_m	Mass mean particle diameter $[m]$
d_{50}	Mass median particle diameter $[m]$
D	Pipe diameter $[m]$
h	Height of a concentration profile in a pipe $[m]$
f	Darcy Weisbach friction factor $[-]$
f_t	Sobota & Krill (1992) coefficient $[-]$
f_ε	Dispersion correction coefficient $[-]$
f_c	Pump head reduction factor $[-]$
F	Solids flux $[m/s]$
g	Gravitational constant $[m/s^2]$
j	Volumetric flux $[m/s]$
k_s	Pipe wall roughness $[m]$
K	Appendage loss factor $[-]$
L_w	Density wave length $[m]$
m	Richardson & Zaki (1954) exponent $[-]$
n	Rotational velocity of a centrifugal pump $[-]$
N	Amount of cells in the numerical domain $[-]$
N_a	Amount of appendages in the numerical domain $[-]$
R_s	Slip ratio $[-]$
Re_p	Particle Reynolds number $[-]$
t	Time $[s]$
u^*	Shear velocity $[m/s]$
u_{crit}	Critical velocity $[m/s]$
u_{dl}	Deposit limit velocity $[m/s]$
u_f	Cross section averaged fluid velocity $[m/s]$
u_r	Relative velocity between the solids and the fluid $[m/s]$
u_s	Cross section averaged solids velocity $[m/s]$
$u_{s/m}$	Particle velocity relative to the volumetric mixture velocity $[m/s]$
u_m	Cross section averaged mixture velocity based on the volumetric flow rate $[m/s]$
$\widehat{u}_m$	Cross section averaged mixture velocity based on the mass flow rate $[m/s]$
v_{ts}	Terminal settling velocity of a particle $[m/s]$
p	Pressure $[Pa]$
p_{man}	Manometric pressure $[Pa]$
Q_s	Volumetrical flow rate of the solids $[m^3/s]$
Q_m	Volumetrical flow rate of the mixture $[m^3/s]$
S_p	Pump pressure gradient source term $[Pa/m]$
S_t	Stokes number $[-]$
t_f	Fluid reaction time $[s]$
t_p	Particle reaction time $[s]$
V	Volume of a grid cell $[m^3]$
x	Directional axial coordinate $[m]$

Amplification through transient accumulation is caused by local particle velocity differences (as a function of pipe orientation) and interaction between the centrifugal pump load and changing pipeline resistance (more details in chapter 2). These interactions are difficult to isolate and study experimentally, since they occur simultaneously and the interaction is two way. Due to the complex nature of the interaction the problem is best investigated using transient modeling. Therefore, this article presents a 1D Driftflux CFD model, which accounts for the pump-pipeline interaction and particle velocity variations and is capable of predicting density wave amplification. The 1D model shows very satisfactory agreement with the Freiberg experiments.

2. Theory - transient accumulation

The mechanism causing density wave amplification at mixture velocities far exceeding the deposit limit velocity, as experienced in the Freiberg experiments, was first discussed in [5]. It was speculated that amplification was caused by a velocity difference of particles when flowing from the horizontal into and vertical parts of the circuit. The reasoning was based on studying the Freiberg data, observing that density waves grew faster at lower velocities (but still above the deposit limit) and at higher concentrations, which increases the spatial particle velocity difference. The volumetric mixture velocity

$$u_m = u_s \cdot c + u_f \cdot (1-c) \tag{1}$$

is by its definition spatially constant

$$\frac{\partial u_m}{\partial x} = 0 \tag{2}$$

With u_s = the cross section averaged particle velocity, u_f = the cross section averaged fluid velocity and c = the volumetric concentration of solids. The solids velocity u_s and fluid velocity u_f may change locally, for instance due to the pipe orientation, or a difference in the local mixture concentration. Regardless, u_m remains the same throughout the pipeline, as u_m is based on a volume flow balance. The transport of particles in a pipe can be described with a 1D advection-diffusion equation [3,5,7]:

$$\frac{\partial c}{\partial t} + \frac{\partial}{\partial x}(u_s \cdot c) = \frac{\partial}{\partial x}\left(\varepsilon \frac{\partial c}{\partial x}\right) \tag{3}$$

Where x = the axial coordinate along the pipe (regardless of orientation) and ε = a diffusion coefficient. As mentioned before, the cross section averaged particle velocity u_s can differ locally, as a function of the local concentration and pipe orientation. Particles travel faster in vertical pipes, because frictional losses are lower compared to horizontal pipes. Assuming a temporal steady-state, and the effect of diffusion is low, Eq. (3) reduces to:

$$\frac{\partial}{\partial x}(u_s \cdot c) = 0 \tag{4}$$

As such, when particles flow from a vertical riser into a horizontal pipe and the particle velocity decreases, the concentration increases simultaneously. The particle velocity in the horizontal pipe can be estimated from the slip ratio R_s [8], which is a commonly used concept by hydraulic transport researchers, although it is difficult to measure and therefore data and models are scarce.

$$R_s = \frac{u_s}{u_m} \tag{5}$$

For vertical pipes [7] showed that the cross section average particle velocity u_s can be modeled well using the hindered settling principle [9], under the assumptions that the particles are homogeneously

distributed in the pipe cross-section, which is typically the case at high concentration ($c > 0.03$) [10]:

$$u_s = u_m - v_{ts} \cdot (1-c)^m \cdot 10^{-d/D} \tag{6}$$

In the Equation above v_{ts}= the terminal settling velocity of a particle and m= the Richardson & Zaki settling exponent (calculated using [11]). The terminal setting velocity can be calculated using [12].

Fig. 1 shows the ratio of the particle velocity u_s over the volumetric mixture velocity u_m as a function of u_m at a volumetric concentration of $c = 0.15$, for a vertical riser and a horizontal pipe. For the horizontal pipe the slip ratio model from [13] was used (for more details see chapter 3.2).

The magnitude of the particle velocity difference between the vertical and horizontal pipes is shown well in Fig. 1. The spatial particle velocity difference is higher at lower mixture velocities. Thus from this trend, if amplification is indeed caused by a spatial particle velocity change, one expects that amplification would be more severe at lower mixture velocities, which was indeed observed in the Freiberg experiments (more details in chapter 3.1).

However, [5] does not manage to explain how a spatial velocity change actually leads to amplification of density waves. Imagine a vertical riser, followed by a horizontal pipe and another riser. At a constant mixture velocity, a density wave first flows from the riser into the horizontal pipe. As a results, the particle velocity decreases going from (1) to (2) in Fig. 1, accompanied by an increase in concentration. Once the mixture flows out of the horizontal pipe and into the second riser, the mixture velocity increases (from (2) to (1) in Fig. 1) and the concentration recovers. The transient accumulation in the horizontal pipe was temporary.

However, if the mixture velocity increases when the density wave flows through the horizontal pipe, the concentration recovers less when flowing into the second riser, from (3) to (4) in Fig. 1. In other words, when the mixture velocity increases, the spatial particle velocity change is less when the wave flows out of the horizontal pipe compared to when the wave flowed into the horizontal pipe. Mathematically, the absolute value of the spatial velocity gradient when the wave flows from the first riser (1) into the horizontal pipe (2), is greater than the gradient when the wave flow out of the horizontal pipe (3) into the second riser (4), if the mixture velocity accelerates when the wave was flowing through the horizontal pipe:

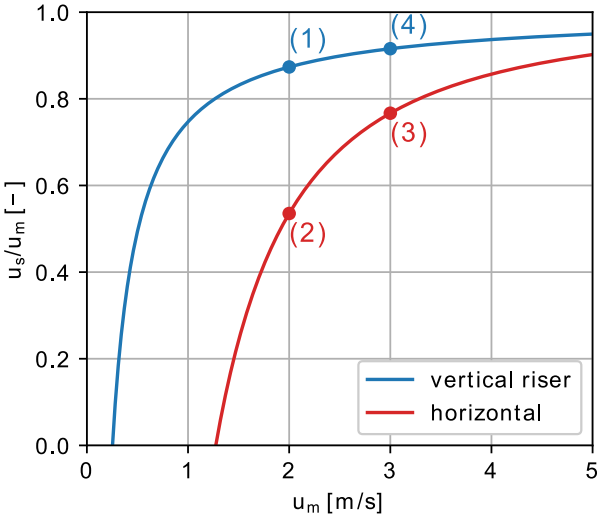

Fig. 1. The cross section averaged particle velocity in a vertical riser and a horizontal pipe, calculated using Eqs. (24) and (6). $D = 150\,mm$, $d = 11.2\,mm$, $\rho_s = 2650\,kg/m^3$, $c = 0.15$.

$$\left|\left(\frac{\partial u_s}{\partial x}\right)_{1,2}\right| > \left(\frac{\partial u_s}{\partial x}\right)_{3,4} \tag{7}$$

and

$$\left(\frac{\partial c}{\partial x}\right)_{1,2} > \left|\left(\frac{\partial c}{\partial x}\right)_{3,4}\right| \tag{8}$$

if

$$\left(\frac{\partial u_m}{\partial t}\right)_{2,3} > 0 \tag{9}$$

Note that the concentration of the wave does not increase when flowing through the horizontal pipe, because there is no spatial velocity change (caused by a pipe orientation change) and only a temporal mixture velocity change (i.e. $\frac{\partial u_s}{\partial x} = 0$).

Concluding, when the mixture accelerates the mixture concentration does not recover to its original when the wave flow out of the horizontal pipe and the density wave remains amplified. The mixture velocity increases when the density wave flows into the horizontal pipe, because a centrifugal pump does not operate at constant flow rate, and the hydrostatic pressure required to lift the wave in the riser is lost. As such, the system accelerates while the pump revolutions remain constant.

3. Methods and materials

3.1. Experiments

In 2017 a vertical hydraulic transport flow loop was constructed in a vertical mineshaft by a collaboration of Royal IHC and Bergakademie Freiberg located in Halsbücke, Germany. The goal of this flow loop was to investigate and validate wall resistance models, particle slip models, plug formation for vertical hydraulic transport used for deep sea mining applications. The flow loop, with a 152 *mm* inner diameter, consisted of a 121 *m* vertical descending pipe, a 121 *m* long riser and 57 *m* of horizontal pipelines at the top side. The top side pipes were to facilitate the centrifugal pump and the soil injection and separation equipment. See Fig. 2 for a schematic overview of the flow loop and the instrumentation. For more details a reference is made to [6].

The flow loop was instrumented with a magnetic flow meter (Krohne Optiflux 4000) to measure the mixture velocity, a pressure differential meter measuring the centrifugal pump manometric pressure and a u-loop delivered concentration measurement system [14]. The delivered concentration

$$c_{vd} = \frac{Q_s}{Q_m} \tag{10}$$

is defined as the ratio of the solids flow rate Q_s over the mixture flow rate Q_m [8] and is measured based on differential pressure according to the technique described in [14]. The corresponding differential pressure measurement over $p1 \rightarrow p2$ and $p3 \rightarrow p4$ was placed $7.5\,m$ apart at the bottom of the two vertical pipes, see Fig. 2.

The researchers used sand and gravel with a d_{50} particle diameter of $600\,\mu m$ and $11.2\,mm$ respectively (distribution in Fig. 3) and the volumetric concentration of sediment was varied as an experimental parameter, between 0.05 and 0.15. The deposition limit velocity of these two sediment types was estimated to be ~$2.5\,m/s$ and ~$1.5\,m/s$, for the $600\,\mu m$ sand and $11.2\,mm$ gravel respectively. The mean particle diameter

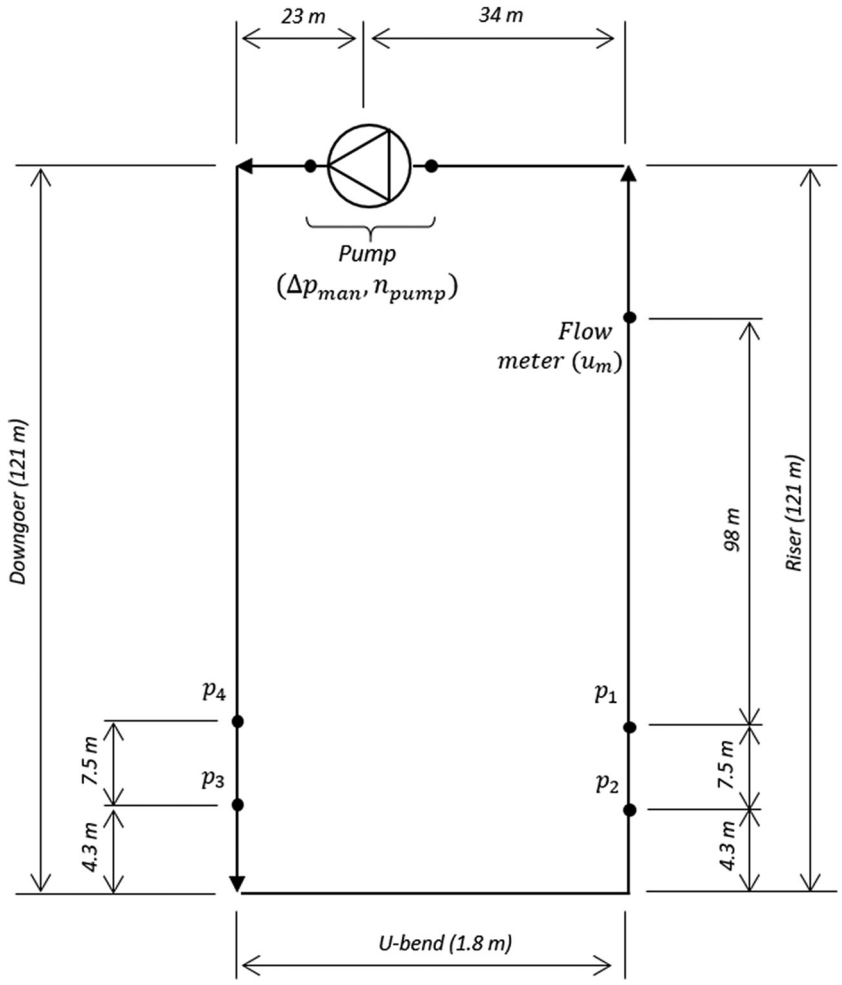

Fig. 2. A schematic of the flow loop built in Freiberg.

$$d_m = \frac{d_{10} + d_{20} + \ldots + d_{90}}{9} \tag{11}$$

of the sand and gravel are $d_m = 741\,\mu m$ and $d_m = 12.1\,mm$, respectively.

The experiments were set up to measure the steady state pressure losses of the mixture. As such, the test started at the highest velocity, thereafter the velocity was lowered in increments of $0.5\,m/s$ every few minutes. The results of four notable experiments can be viewed in Figs. 4, 5, 6 and 7, showing time traces of the mixture velocity, delivered concentration, pump pressure and pump revolutions. At the start of the experiment the system was empty, as shown by the concentration time traces, and was filled up to the desired sediment concentration. Each experiment was preceded by a water experiment, which were used to determine wall friction coefficients. The relative wall roughness $\frac{k_s}{D}$ changed throughout the course of the experimental program, varying between $4.7{\cdot}10^{-4} \leq \frac{k_s}{D} \leq 9.5{\cdot}10^{-4}$.

The density wave amplification effect is clearly demonstrated in Figs. 4, 5, 6 and 7 and occurred in all conducted experiments. No additional sediment was added and the system was a closed loop, therefore amplification is in essence a material redistribution effect. Also note that

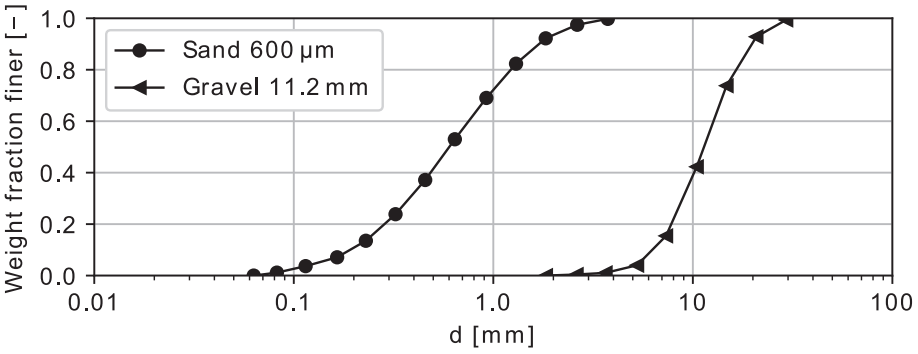

Fig. 3. The particle size distribution of the 600 μm sand, and the 11.2 mm gravel.

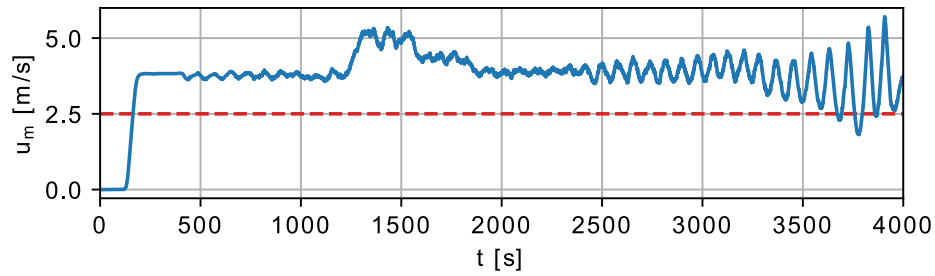

(a) Blue solid: The measured mixture velocity. Red dashed: estimation of u_{dl}.

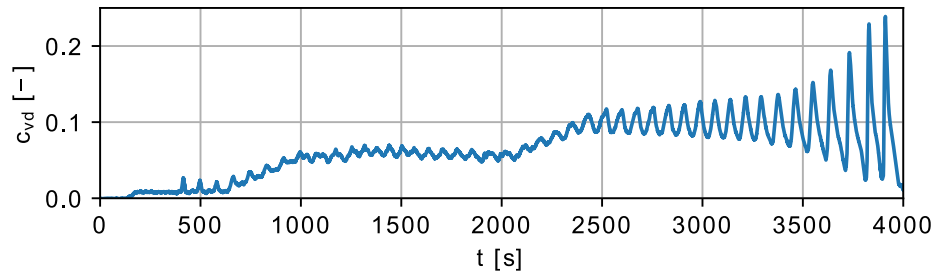

(b) The delivered concentration.

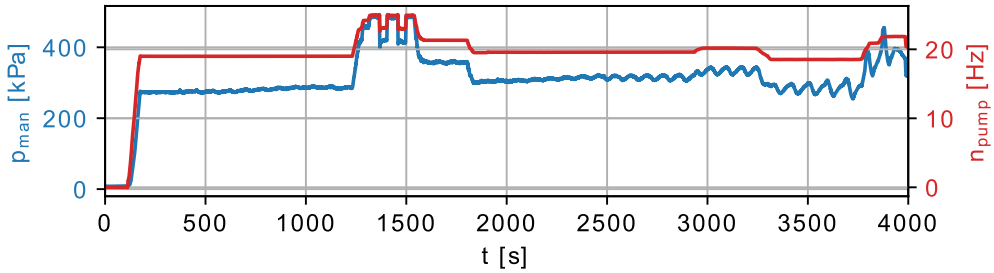

(c) The pump manometric pressure (blue) and the pump revolutions (red).

Fig. 4. Experiment nr. 1, with sand, $d_m = 741\mu m$, $c = 0.05 - 0.10$.

amplification occurred even when the pump revolutions were constant over long periods. Also notable is the fact that the mixture velocity at which amplification took place was well above the deposit limit velocity, which is a stability criterion to avoid amplification through the erosion and sedimentation imbalance as described in [5]. The threshold velocity at which the first significant wave was formed (which continues to grow) is given in Table 1 as u_{th}, which is between 40% and 110% higher than the deposit limit velocity. In addition the wave length of the density waves was roughly equal to the system length (the total length of all pipes). Furthermore, the shape of strong density waves is saw-tooth like (Figs. 4b and 7b) and skewed towards the front of the wave. The saw-tooth shape is caused by the fact that at high concentration the cross section averaged particle velocity is higher than at low concentration [4,5].

The mixture velocity varies in unison with the density waves. This is a result of the working principle of a centrifugal pump. Namely, the mixture velocity is a result of both the pump revolutions and the resistance of the pipeline [8]. At constant pump revolutions, the pipeline resistance continues to change and depends on the position of the density wave in the pipeline. The pipeline resistance is highest when the density wave travels up the riser, due to the hydrostatic mixture gradient. And the resistance is lowest when the wave travels down the downgoer and the hydrostatic gradient accelerates the mixture. When the waves flows out of the riser into the horizontal pipes, the mixture accelerates and the conditions are met to initiate amplification through the transient accumulation mechanism as explained in chapter 2.

The experiment shown in Fig. 4 was initially at an average volumetric delivered concentration $c_{vd} = 0.05$, and small waves were constant in amplitude, however once the system was filled further up to $c_{vd} = 0.10$ the density wave grew with each circulation through the loop, while the average mixture velocity had not changed significantly ($u_m \approx 3.7 m/s$), but still remained well above the deposit limit velocity ($u_{dl} \approx 2.5 m/s$). This demonstrates that the concentration influences the onset of amplification and the amplification rate. This concentration dependency is further demonstrated in the experiments of Figs. 6 and 7, where $11.2\,mm$ gravel was transported at an average volumetric concentration of 0.05 and 0.15, respectively. The low concentration experiment was initially stable, until the mixture velocity was reduced to around $u_m = 2.5 m/s$ and amplification sets on very rapidly, while still being above the deposit limit velocity $u_{dl} \approx 1.5 m/s$. The high concentration gravel experiment however (Fig. 7) was unstable from the start ($u_m \approx 3.2 m/s$, $u_{udl} \approx 1.5 m/s$), regardless of the high velocity, demonstrating the concentration influence on amplification. Chapter 2 explains how density waves can amplify due to a spatial particle

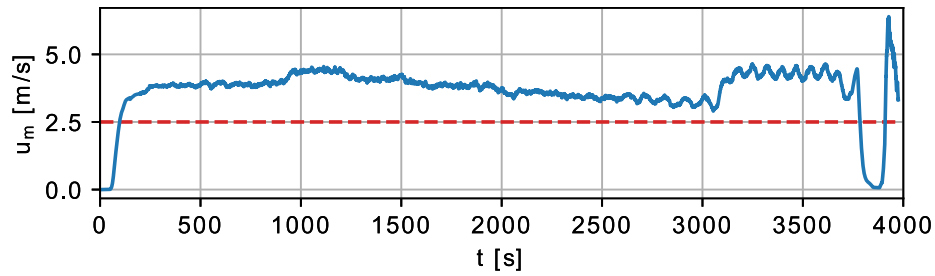

(a) Blue solid: The measured mixture velocity. Red dashed: estimation of u_{dl}.

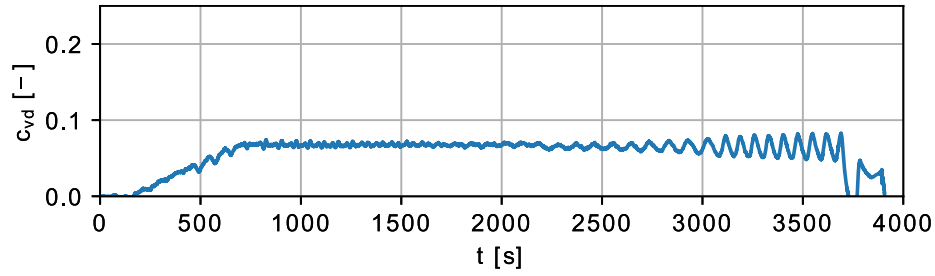

(b) The delivered concentration.

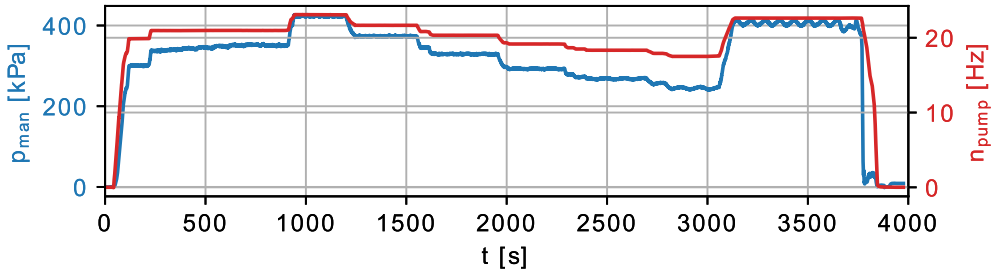

(c) The pump manometric pressure (blue) and the pump revolutions (red).

Fig. 5. Experiment nr. 2, with sand, $d_m = 741\mu m$, $c = 0.07$.

velocity change. The magnitude of the velocity change is a function of the concentration, being larger at higher concentration. A larger spatial velocity change therefore leads to a higher amplification, which explains the concentration dependency amplification.

Figs. 5 and 6 also demonstrate that the average mixture velocity influences the onset of amplification as both experiments were stable at high velocity, and amplification started below a certain velocity, even though the mixture velocity was still well above the deposit limit velocity (~2.5 m/s and ~1.5 m/s, for the 600μm sand and 11.2 mm gravel respectively). This can again be explained because at lower mixture velocities, the spatial velocity change of particles between the horizontal and vertical pipes, is higher than at high velocity. As such the concentration change is also higher at low mixture velocities (see Fig. 1).

3.2. 1D CFD Driftflux model

A 1D CFD Drift-flux model is proposed to study and model the density wave amplification as witnessed in the Freiberg flow loop. For the model to predict density wave amplification, the particle velocity should be a function of pipe orientation (vertical or horizontal) and of the concentration (see chapter 2). Furthermore, the model should be pressure driven and the pressure source should be representative of a centrifugal pump, where the pressure is a function of the volumetric flow rate, particle diameter and concentration. With such a pressure driven model, the variations in pipeline resistance will lead to mixture velocity variations.

3.2.1. Model structure

For the 1D model presented below all scalar values are cross section averaged values. In the Driftflux model a distinction is made between two types of mixture velocities. The first mixture velocity u_m is based on the volumetric flow rate of all phases (Eq. (1)). Another mixture velocity $\hat{u}_m$ can be defined based on the mass flow rate of the phases [15]:

$$\hat{u}_m = u_f \cdot \frac{\rho_f}{\rho_m} \cdot (1-c) + u_s \frac{\rho_s}{\rho_m} \cdot c \tag{12}$$

With ρ_s= the solids density, ρ_f= the fluid density phase density and ρ_m= mixture density. u_m is often referred to as the volumetric flux j and $\hat{u}_m$ the Favre average mixture velocity in Drift-flux literature [15,16]. The Drift-flux model is based on a single continuity equation taking into account all phases [15,16]:

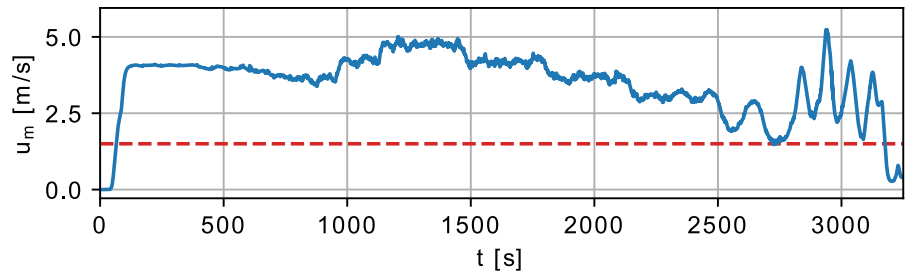

(a) Blue solid: The measured mixture velocity. Red dashed: estimation of u_{dl}.

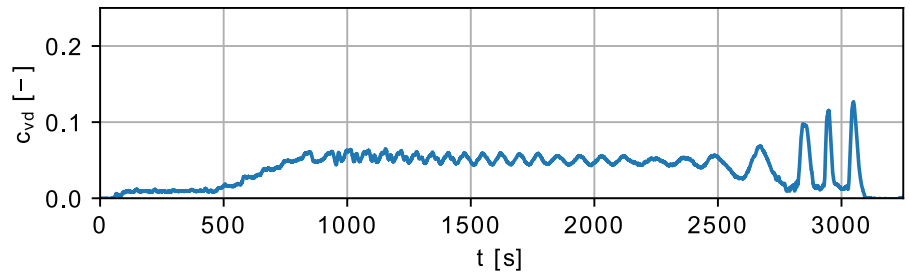

(b) The delivered concentration.

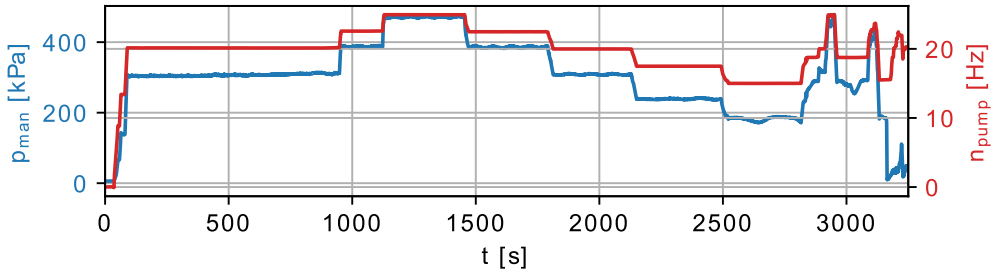

(c) The pump manometric pressure (blue) and the pump revolutions (red).

Fig. 6. Experiment nr. 3, with gravel, $d_m = 12.1\,mm$, $c = 0.05$.

$$\frac{\partial \rho_m}{\partial t} + \frac{\partial}{\partial x}\left(\rho_m \cdot \hat{u}_m\right) = 0 \tag{13}$$

The 1D mixture momentum equation is based on the assumption that the mixture can be modeled as a single fluid with density ρ_m and is based on the work of [7,16]. Note that x is the axial coordinate along the pipeline, whether the pipe is horizontal or vertical.

$$\begin{aligned}\frac{\partial}{\partial t}\left(\rho_m \cdot \hat{u}_m\right) + \frac{\partial}{\partial x}\left(\rho_m \hat{u}_m |\hat{u}_m|\right) = &-\frac{\partial p}{\partial x} + \frac{4\tau_m}{D} + \rho_m g \cos(\omega) + \dots \\ &\frac{\partial}{\partial x}\left[c\rho_s\left(\hat{u}_m - u_s\right)^2 + (1-c)\rho_f\left(\hat{u}_m - u_f\right)^2\right] + S_p\end{aligned} \tag{14}$$

In Eq. (14), τ_m= mixture wall shear stress, ω= pipe inclination angle ($\omega = 0 \vee \omega = \pm\,\pi/2$), S_p = a pressure gradient source term to model the pressure added by a centrifugal pump and the second from last term represents the inertial coupling forces, caused by a velocity difference between the phases [17–19]. Pipes at different orientation (currently only vertical or horizontal) can be modeled by specifying an inclination angle for each grid cell, and as such vertical and horizontal pipes can be modeled in the same domain and solving a single momentum equation. In theory any pipe inclination could be modeled with Eq. (14), however certain closure relationships need to be adapted to be valid for all inclinations (see below). Currently the closures presented in this work are only for horizontal and vertical pipes.

The particle transport is modeled using the finite volume method, which is best to ensure mass continuity. Since with a 1D model, small mass discontinuities are very noticeable. The finite volume method according to [20]:

$$\int_V \frac{\partial c}{\partial t} dV + \oint_A \vec{F} \cdot d\vec{A} = 0 \tag{15}$$

Where c = the volumetric concentration, V = the volume of a finite volume, F = the solids flux and A = the volume surface. Using the 1D grid definition shown in Fig. 8, allows us to rewrite Eq. (15) to:

$$\frac{\partial c}{\partial t} + \frac{1}{\Delta x}\sum_{faces} F = 0 \tag{16}$$

With F = the cell face solid fluxes.

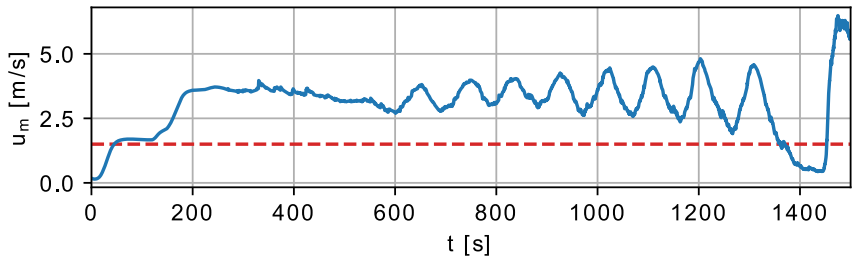

(a) Blue solid: The measured mixture velocity. Red dashed: estimation of u_{dl}.

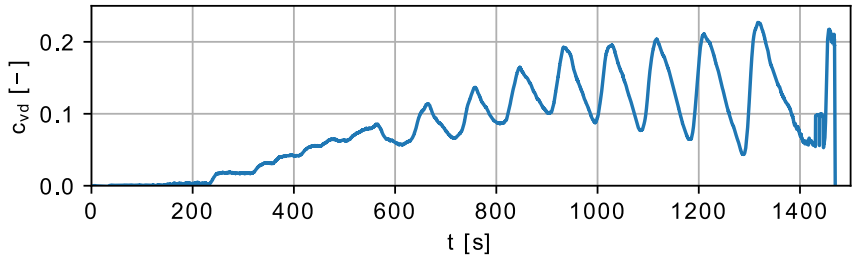

(b) The delivered concentration.

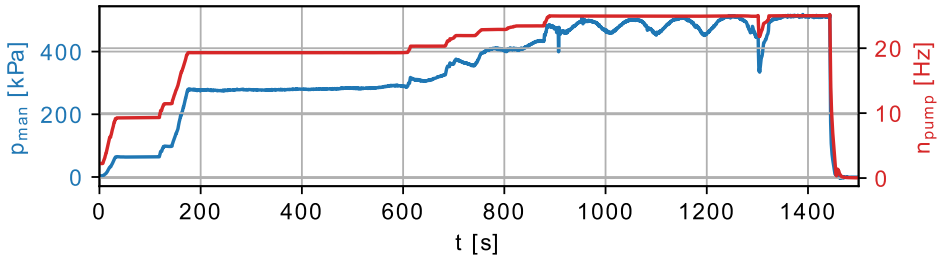

(c) The pump manometric pressure (blue) and the pump revolutions (red).

Fig. 7. Experiment nr. 4, with gravel, $d_m = 12.1\,mm$, $c = 0.14$.

The cell face solid fluxes are modeled as:

$$F = u_s \cdot c \tag{17}$$

Typically the model is advection dominated, therefore to ensure stability c is numerically modeled using the van Leer flux limiter [20]. The particle cross section averaged particle velocity u_s is modeled as:

$$u_s = u_m + u_{s/m} - \frac{\varepsilon}{c} \cdot \frac{\partial c}{\partial x} \tag{18}$$

Where $u_{s/m}$ is the cross section averaged relative velocity of the particle with respect to the volumetric mixture velocity u_m and the last term Eq. (18) is the diffusion velocity, modeled through the diffusion coefficient ε (note: $u_{s/m}$ is negative if the particle velocity is lower than the mixture velocity).

Table 1
Parameters of the conducted experiments.

nr.	$d_m[mm]$	$d_{50}[mm]$	$c[-]$	$u_{dl}[m/s]$	$u_{th}[m/s]$
1	0.741	0.600	0.05–0.10	~2.5	~3.7
2	0.741	0.600	0.07	~2.5	~3.5
3	12.1	11.2	0.05	~1.5	~2.5
4	12.1	11.2	0.14	~1.5	~3.2

3.2.2. Closure relationships

The 1D Driftflux model as presented above requires relationships for the wall shear stress τ_m, the relative particle velocity $u_{s/m}$ and the diffusion coefficient ε. The wall shear stress of the mixture is the sum of the wall shear stress caused by the fluid τ_f, by the solids τ_s and minor losses τ_{ml} from system components like bends and flanges:

$$\tau_m = \tau_f + \tau_s + \tau_{ml} \tag{19}$$

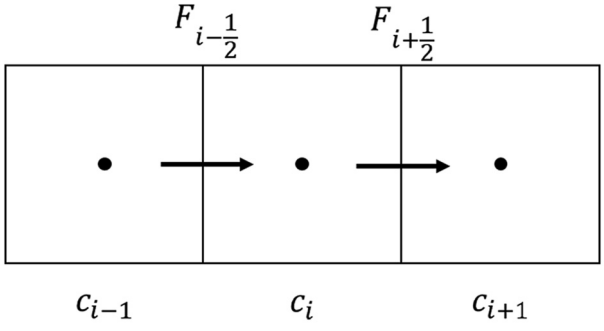

Fig. 8. The grid definition of the 1D Drift-flux model.

The fluid shear stress is calculated using the Darcy-Weisbach equation:

$$\tau_f = \frac{f}{8}\rho_f u_m^2 \tag{20}$$

With f = Darcy-Weisbach friction factor, ρ_f the fluid density. Minor losses are to account for losses from appendages (bends, flanges and valves). The minor losses are in practice local losses, but in the solver are distributed over the entire domain, to avoid and excess amount of large pressure gradients, and associated numerical stability issues.

$$\tau_{ml} = \frac{1}{N}\sum_{i=0}^{N_a-1} K_i \frac{D}{8}\rho_{m,i} u_{m,i}^2 \tag{21}$$

With K_i = the appendage loss coefficient, N = the amount of cells in the 1D domain, N_a = the amount of appendages, $\rho_{m,i}$ = the local mixture density at the appendage and $u_{m,i}$ = the local mixture velocity. The solids shear stress for sand can be modeled with the equivalent liquid model concept for sufficiently high mixture velocities [8]. For sand and horizontal pipes the wall friction is calculated as:

$$\tau_s = \frac{f}{8}\left(\rho_m - \rho_f\right)u_m^2 \tag{22}$$

With ρ_m = mixture density and ρ_f = the fluid density. This wall sheer stress model is valid for sand slurries at high velocities ($u_m >> u_{dl}$), which is valid when applying this model for the Freiberg experiments. However, for more general cases (other than this research) keep in mind that a wall resistance model might be needed which is better suited at mixture velocities close to the deposit limit velocity, such as wall resistance models for heterogeneous slurries [21]. For the gravel slurries the wall friction is significantly higher compared to sand slurries, as the sediment is transported in a sliding bed layer. Therefore we recommend to use the sliding bed correlation used by [22–24]. For gravel and horizontal pipes the wall friction is calculated as:

$$\tau_s = \mu_{sf}\frac{D}{4}g\left(\rho_m - \rho_f\right) \tag{23}$$

With μ_{sf} = the mechanical friction factor between the sliding gravel bed and the pipe wall ($\mu_{sf} \approx 0.4$), D = the pipe diameter, g = the gravitational constant. This sliding bed wall friction model can be improved by applying more advanced stationary two-layer models for sliding bed flow [8,25], however these are iterative in nature. Furthermore, these iterative models were found to be difficult to implement in within this numerical framework, due to instabilities in the two-layer model results and vastly increased calculation times. The focus of this research was on developing the 1D model framework, therefore we use a less accurate, but easier to use empirical model (Eq. (23)). For vertical pipes Eq. (22) is applied to model the wall friction, which is valid for vertical flows if the distribution of particles in the pipe cross section is homogeneous and mechanical stresses due to particle-wall contact is low.

The relative velocity $u_{s/m}$ models the velocity difference between the solids and the mixture. Empirical slurry transport research focuses mostly on wall friction losses, yet some measurements and relationships of the slip ratio (Eq. (5)) have been made during the past decades. The state of the art are physical stationary two-layer models [8,25], but again these models require iterative computation. As part of this research the empirical correlation of [13] was found to be a good alternative to simulate both sand and gravel slurries in horizontal pipes, as this model was calibrated for both sand and gravel flows. The relative velocity is calculated from the slip ratio as:

$$u_{s/m} = u_m(R_s - 1) \tag{24}$$

In the Equation above R_s is modeled according to [13]:

$$R_s = 1 - f_t \cdot \left(1 - \frac{c}{c_{max}}\right)^{2.16} \cdot \left(\frac{u_{crit}}{u_m}\right)^{1.7} \tag{25}$$

In which c_{max} = the maximum concentration of the sediment ($c_{max} \approx 0.6$) and u_{crit} = the critical velocity. [13] does not provide a definition of u_{crit}, however in slurry transport research u_{crit} and u_{dl} typically describe a similar threshold velocity, the transition between particles in suspension and particle settling out of suspension ($u_{crit} \approx u_{dl}$). The empirical constant f_t was provided by [13] as a graph as a function of $\log(Re_p)$. The Reynold particle number

$$Re_p = \frac{d \cdot v_{ts}}{\nu_f} \tag{26}$$

is a function of the particle diameter d, the terminal settling velocity v_{ts} and the fluid viscosity ν_f. f_t can be approximated using:

$$f_t = \begin{cases} 0.1464 \cdot 10^{0.6031 \cdot \log\left(Re_p\right)} & \text{if } \log\left(Re_p\right) < 1 \\ 0.7858 \cdot \tanh\left[0.7986 \cdot \log\left(Re_p\right)\right] & \text{if } \log\left(Re_p\right) \geq 1 \end{cases} \tag{27}$$

The particle velocity in the vertical pipes is modeled according to Eq. (6).

The diffusion coefficient ε is modeled using Taylor dispersion [26]:

$$\varepsilon_{Taylor} = 10.1 \cdot \frac{D}{2} \cdot \sqrt{\frac{\tau_f}{\rho_f}} \tag{28}$$

With D = pipe diameter, τ_f = the fluid wall friction and ρ_f = the fluid density. In [7,27] it was found that large particles experience reduced axial dispersion due to their higher inertia, and are therefore affected less by turbulent hydrodynamic forces. A modification to Taylor dispersion was proposed by [7], as a function of the Stokes number St:

$$\varepsilon = \varepsilon_{Taylor} \cdot f_\varepsilon \tag{29}$$

$$f_\varepsilon = \begin{cases} 1 - \frac{2}{3} \cdot St & \text{if } 0 < St \leq 1.5 \\ 0 & \text{if } St > 1.5 \end{cases} \tag{30}$$

The Stokes number is used to judge how well a particle is able to follow changes in the fluid velocity field and is a ratio of the particle reaction time t_p over the fluid reaction time t_f.

$$St = \frac{t_p}{t_f} \tag{31}$$

If $St << 1$ particle follows the fluid well and if $St >> 1$ particles detach from the flow. A suggested method to compute the Stokes number of large particles is given by [7,27]:

$$St = \frac{4 \cdot \left(\rho_s - \rho_f\right) \cdot d \cdot u_m}{3 \cdot \rho_f \cdot D \cdot v_{ts} \cdot C_D} \tag{32}$$

With ρ_s = particle density and C_D = the drag coefficient of a particle.

3.2.3. Implementation of a centrifugal pump

The centrifugal pump pressure is implemented in the momentum equation through the pressure gradient source term S_p. The source term can be applied in one grid cell, adding a pressure gradient representative of the pressure provided by the centrifugal pump. This method also supports multiple pump pressure sources along the domain, to simulate a multi-pump pipeline.

$$S_p = \frac{\Delta p_{man}}{\Delta x} \tag{33}$$

In the Equation above p_{man} = the manometric pressure added by the centrifugal pump, and Δx = the grid cell width. The manometric pressure of the pump is a function of the pump flow rate, this relationship is provided by the pump diagram. Fig. 9 gives the pump diagram of the pump used in the Freiberg flow loop, and was determined by measurement.

The input of the 1D Driftflux is the rotational velocity of the pump. The pump curve of Fig. 9 is scaled to the desired rotational velocity according to the following affinity laws [8]:

$$\frac{Q_n}{Q_0} = \frac{n}{n_0} \tag{34}$$

$$\frac{p_{man,n}}{p_{man,0}} = \left(\frac{n}{n_0}\right)^2 \tag{35}$$

In the above Q_n and $p_{man,n}$ are the flow rate and the manometric pressure of the centrifugal pump at revolutions n, respectively. Q_0 and $p_{man,0}$ are the respective flow rate and manometric pressure at reference revolution $n_0 = 24.66Hz$, see Fig. 9.

The pressure of the pump increases proportionally with the local mixture density. However, this increase reduces slightly due to additional frictional losses caused by the particles. The pump head reduction factors of Stepanoff [28] are applied to correct for these additional losses as shown in the Equation below.

$$\frac{p_{man,m}}{p_{man,f}} = \frac{\rho_m}{\rho_f} f_c \tag{36}$$

With $p_{man,m}$ = the pump manometric pressure at mixture density ρ_m and $p_{man,f}$ = the pump pressure at the fluid density ρ_f, and f_c = the Stepanoff head reduction factor.

$$f_c = 1 - c_{vd}[0.8 + 0.6 \cdot \log(d)] \tag{37}$$

In the Equation above c_{vd} is the delivered concentration and d the particle diameter (d in $[mm]$).

3.2.4. Numerical implementation

The 1D Driftflux model of this research is an in-house research code and closely follows the discretization and solving techniques as described by [7,16]. Summarized: The momentum equation (Eq. (14)) was discretized on a staggered mesh. The Adams-Bashfort two time integration scheme [20] was applied to calculate an intermediate momentum, to allow for the large pressure gradients caused by the centrifugal pump source term (S_p is applied in a single cell, resulting in a large pressure gradient). The results thus far obtained were used together with the fractional step method, giving a Pressure Poisson equation, which is solved using the Thomas algorithm. The momentum of the new time step is computed from the newly acquired pressure field, which also allows for computation of the mass based mixture velocity $\hat{u}_m$ on the new time step.

From the updated mass based mixture velocity $\hat{u}_m$, the volumetric mixture velocity u_m is updated, which is required to solve the transport equation. Firstly the relative velocity u_r is computed, which is the difference between the velocity of the solids and fluid phases [15]:

$$u_r = \frac{u_{s/m}}{1-c} \tag{38}$$

The relative velocity is a function of the volumetric concentration c and of the solids velocity relative to the volumetric mixture velocity $u_{s/m}$ (Eq. (24)), which is the closure relationship as explained earlier and can be measured experimentally in laboratory circuits. The volumetric mixture velocity u_m is computed as [15]:

$$u_m = \hat{u}_m + (1-c) \cdot c \cdot \frac{\rho_f - \rho_s}{\rho_m} u_r \tag{39}$$

The solids velocity u_s and the fluid velocity u_f are computed as follows [15]:

$$u_s = u_m + c \cdot u_r \tag{40}$$

$$u_f = u_m - (1-c) \cdot u_r \tag{41}$$

With u_m known, the transport equation can solved using the finite volume method combined with the van Leer flux limiter for stability, as the transport equation is typically advection dominated.

4. Results

The interplay between spatial particle velocity, centrifugal pump load and mixture velocity changes can quickly become very complex and is difficult to investigate experimentally. The 1D Driftflux model presented in this research has the ability to simulate these effects, and investigate the magnitude of the influence of the aforementioned processes on density wave amplification, and therefore validate the hypothesis of transient accumulation.

The results of simulations using the 1D Driftflux model are presented in Figs. 10, 11, 12 and 13. These figures compare the measured and simulated time traces of the volumetric mixture velocity, the delivered concentration and the pump manometric pressure.

4.1. Determination of model parameters

The closure relationships require two parameters, the wall roughness k_s (for the wall friction model) and the critical velocity u_{crit} (for the horizontal relative particle velocity model). All other parameters, such as particle diameter, pipe diameter, particle density, pump characteristics, etc. are known and can directly be applied. The initial conditions of the simulations were determined from the concentration

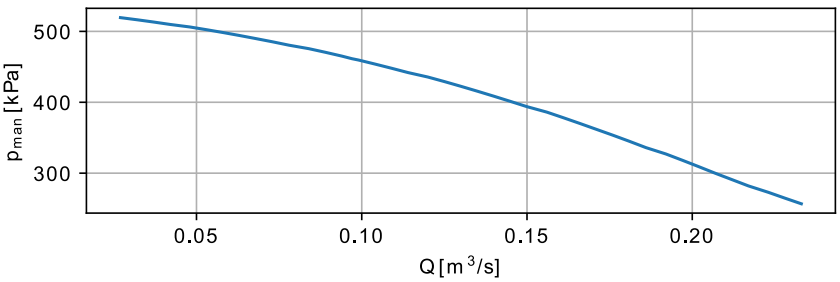

Fig. 9. The pump curve (for water) of the 150 mm centrifugal dredge pump used in the Freiberg experiments, at a rotational velocity of 24.66 Hz.

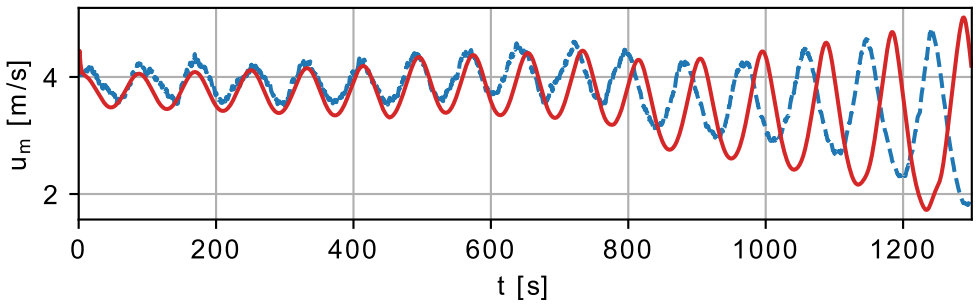

(a) The measured mixture velocity.

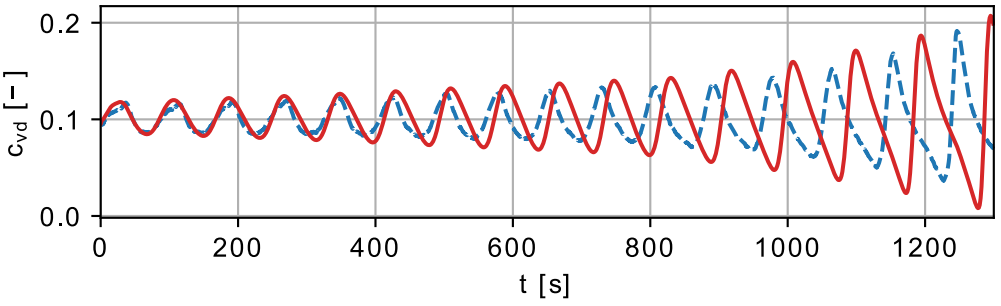

(b) Delivered concentration.

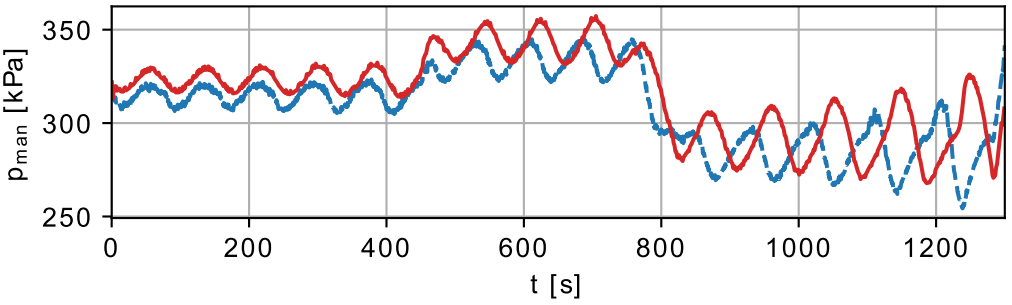

(c) Pump manometric pressure.

Fig. 10. Simulation of the Freiberg experiment nr. 1. Blue: data, red: simulation. Sand, $d_m = 741\,\mu m$, $c = 0.05 - 0.10$.

data, i.e. the first wave in the data was matched with a sinusoidal wave with a mean concentration $\bar{c}$ and an amplitude c', see Table 2. The first simulated wave is typically the first wave after the system was filled with sediment up to the desired concentration.

The wall roughness k_s was determined from the experimental data using a steady state analysis. The experimentally measured pump pressure equals the total resistance losses of the pipe circuit, under steady-state conditions. Therefore, water experiments proceeding each mixture experiment were used to determine the wall roughness for the entire system (excluding minor losses), the results are shown in Table 2. Minor losses calculated based on the amount of bends, valves and flanges in the circuit, resulting in a total of $\Sigma K = 2.81$. The solids frictional losses were modeled as described in chapter 3.2. In case of gravel, the mechanical friction factor between the sliding bed and pipe wall was chosen to be $\mu_{sf} = 0.4$, a typical value [23].

The modeled pump pressure was compared to the predicted pump pressure also using a steady-state analysis. The pump diagram in Fig. 9 was measured accurately in a laboratory in the past, and the particle correction by [28] was found to work very well.

The value of u_{crit} ($\approx u_{dl}$) influences the relative particle velocity model $u_{s/m}$ in the horizontal pipes and therefore influences the simulated amplification rate. Since the relative velocity model for horizontal pipes is not exactly determined for this system and a model from literature is used, some inconstancy between the data and the simulations was experienced when using the values of the estimated deposit limit velocity for u_{crit} ($1.5 m/s$ and $2.5 m/s$ for sand and gravel, respectively). Therefore, the chosen value for u_{crit} was varied slightly to attain a better agreement with the data. The resulting values of u_{crit} used for each experiment are given in Table 2.

To judge how sensitive the results are to inaccuracies in the horizontal relative velocity model, the value of u_{crit} is varied $+/-$ 10% in the simulation of experiment 1, see Fig. 14. Fig. 14 shows that the amplification rate is indeed influenced slightly, however amplification is still predicted. Amplification ceases when choosing $u_{crit} = 1.6 m/s$ (-30%), and for a $u_{crit} = 2.7 m/s$ ($+17\%$) the simulation cannot be completed, because the minimum concentration of the density wave drops below zero. The effect of the variations of u_{crit} on the actual value of the relative velocity $u_{s/m}$ is given in Table 3. From this we can

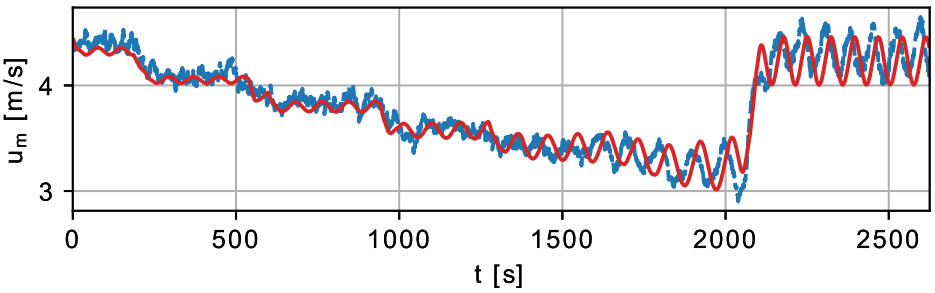

(a) The measured mixture velocity.

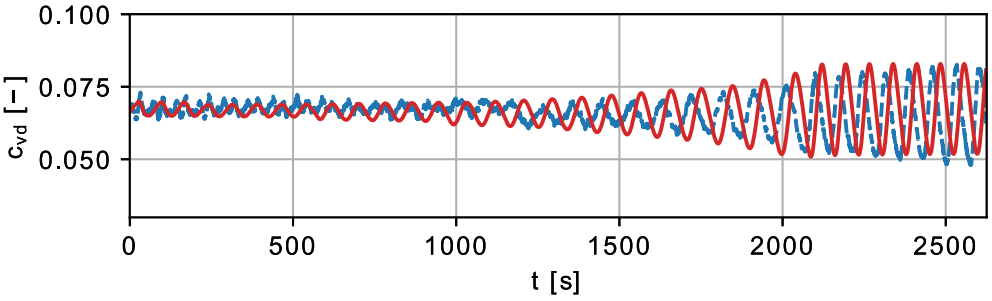

(b) Delivered concentration.

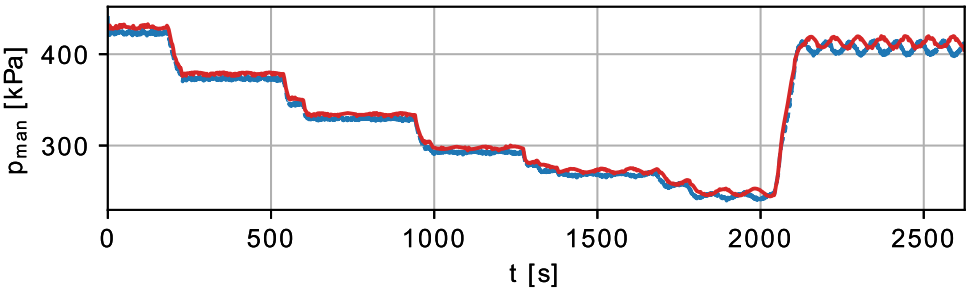

(c) Pump manometric pressure.

Fig. 11. Simulation of the Freiberg experiment nr. 2. Blue: data, red: simulation. S and, $d_m = 741\mu m$, $c = 0.07$.

conclude that to attain representative results in case of experiment 1, in the sense that the model predicts amplification and can finish the simulation, the accuracy of the relative velocity model should be within at least a $+/-$ 15% bandwidth.

4.2. Comparison of the simulation with data

The pump revolutions data of the experiments was used as input for the simulations, together with the initial conditions of the concentration wave. From that point on everything is simulated. Some notable fine details are simulated, like the saw-tooth shape of waves (Figs. 10b, 13b and 14b), caused by the fact that the particle velocity is modeled as a function on the concentration [5]. Furthermore, tiny kinks in the concentration and pump pressure time traces, as seen in Fig. 10 between 1000 and 1200s, can also be seen in the simulations (caused by rapid pump revolutions changes). The simulation of Fig. 12 is very notable, as the system in this experiment could be considered stable up 1050s, even after lowering the mixture velocity several times. However, beyond 1050s a strong density wave sets on rapidly, because the mixture velocity drops below a threshold where the particle velocity difference between the horizontal and vertical pipes becomes very large. This behavior is also simulated very well.

All simulation show an apparent phase shift when comparing the simulations with the data. This is a difference in wave velocity between the data and the simulation. The wave length equals the system length, therefore a slight discrepancy in particle or mixture velocity results in a phase shift as time proceeds. Mixture velocity deviations can be caused by pump pressure or pipe resistance mismatches between the data and simulations. These mismatches could be explained by underperforming resistance or relative velocity models, however also keep in mind that many deviations can originate from the experiments. Especially because the Darcy-Weisbach friction factor is based on the water experiment preceding the mixture experiments, and the wall roughness could change if for instance the pipe erodes during mixture experiments. This also explains the variation in measured wall roughness between the water experiments (see Table 2). In other words the wall roughness changed between experiments, and the water experiment preceding the mixture experiment is not exactly representative of the wall roughness during the mixture experiment. Another cause of mismatches between the data and simulations could come from the

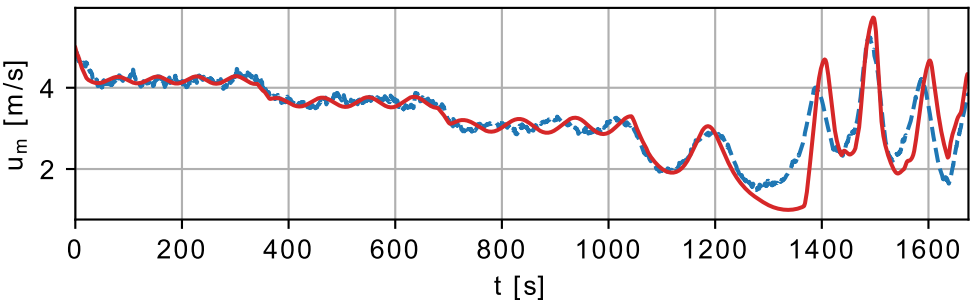

(a) The measured mixture velocity.

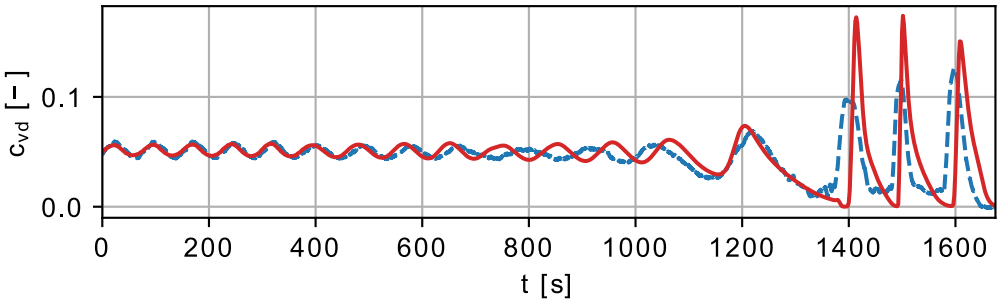

(b) Delivered concentration.

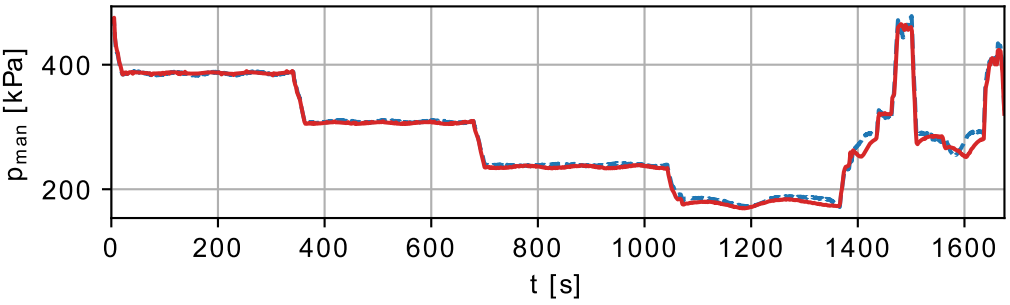

(c) Pump manometric pressure.

Fig. 12. Simulation of the Freiberg experiment nr. 3. Blue: data, red: simulation. Gravel, $d_m = 12.1\,mm$, $c = 0.05$.

delivered concentration measurement with the u-loop measuring principle, which is known to suffer from inaccuracies ($+/-10\%$), especially for coarse sediments [14]. This data serve as input for the model, as such any discrepancies will results in deviations. The wave lengths could be matched better with manual tweaking of the wall friction factor k_s, however this was deliberately not done, to demonstrate that the resulting wave amplification rates are not very sensitive to the aforementioned variations. In the view of the authors the phase lag discrepancy is not an issue, since the 1D model still predicts the amplification rate well.

5. Discussion

The density wave amplification mechanism as witnessed in the Freiberg experiments is new in the sense that amplification can occur at mixture velocities far exceeding the deposit limit velocity, as explained by [5]. However, [5] does not fully explain the transient accumulation mechanism. This article continues this work and provides a hypothesis and relates the mechanism to a spatial particle velocity change with a simultaneous temporal mixture velocity change. The mixture velocity change can also be attributed to the density wave as the mixture accelerates when the wave leaves the vertical riser, which is in its turn caused by the fact that the centrifugal pump does not have a constant operating point. This interaction together with the spatial particle velocity change is modeled with the 1D Driftflux model, and because this model simulates density wave amplification very well, we consider this as proof in support of the transient accumulation hypothesis.

Whether amplification occurs can now be simulated with the 1D Driftflux model. The model can be used to answer some interesting questions. Would amplification occur without the presence of the horizontal pipes? Does the pump position influence amplification. Can amplification be avoided with flow feedback control? Can amplification be avoided by better matching the particle velocity between the horizontal and vertical pipes, by decreasing the diameter of the horizontal pipes. A future study will be dedicated towards these questions.

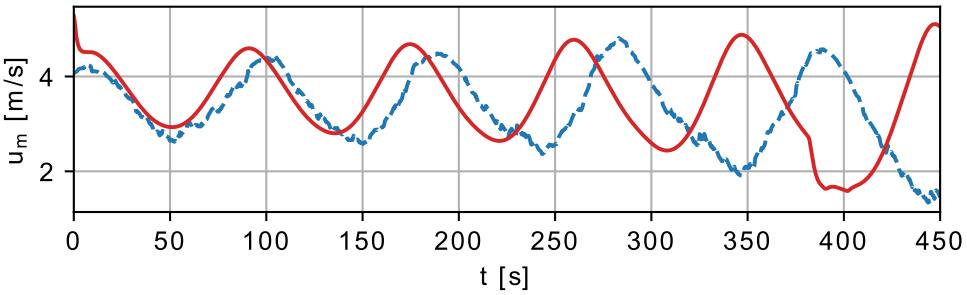

(a) The measured mixture velocity.

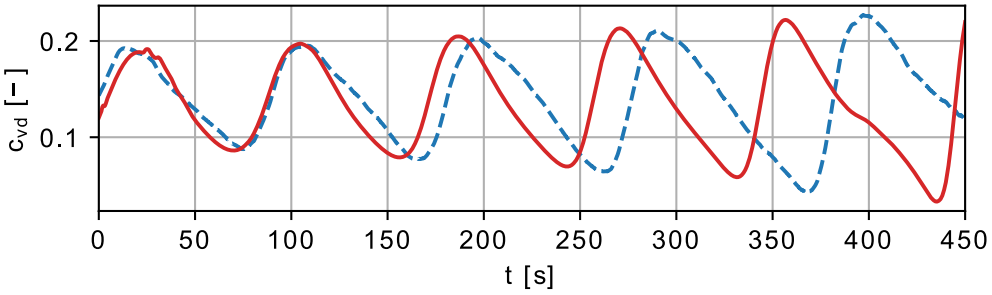

(b) Delivered concentration.

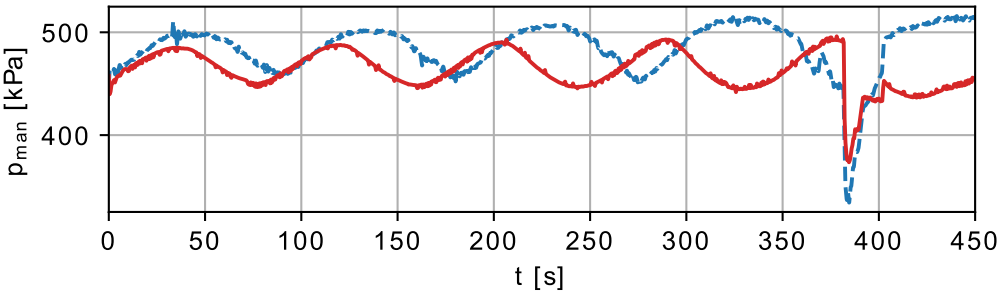

(c) Pump manometric pressure.

Fig. 13. Simulation of the Freiberg experiment nr. 4. Blue: data, red: simulation. Gravel, $d_m = 12.1\,mm$, $c = 0.14$.

The Freiberg flow loop was a closed loop system, while dredging and deep sea mining pipelines are open systems. In the Freiberg loop the wave could amplify during each passing through the loop, which is not possible in an open system. However, the Freiberg data also shows that once the wave is already severe, the growth in one circulation is significant. Therefore, if a strong wave already exists in an open pipeline system, it can amplify when flowing out of a vertical pipe into a horizontal pipe. This can only occur when the system accelerates significantly (see chapter 2), moreover if the vertical pipe is long relative to the horizontal pipe. If a system contains multiple pipe orientation changes, amplification could potentially occur at each transition. To what extent, and how severely transient accumulation affects an open system pipeline requires a more detailed study.

Table 2
For the initial conditions, and k_s and u_{crit} for the simulations.

Exp. #	$d_m[mm]$	$\bar{c}[-]$	$c'[-]$	$\frac{k_s}{D}[-]$	$u_{crit}[m/s]$	$\mu_{sf}[-]$	$c_{max}[-]$
1	0.741	0.10	0.016	$5.1 \cdot 10^{-4}$	2.3	–	0.60
2	0.741	0.067	0.0020	$7.9 \cdot 10^{-4}$	2.2	–	0.60
3	12.1	0.052	0.038	$4.7 \cdot 10^{-4}$	1.8	0.40	0.60
4	12.1	0.14	0.050	$9.5 \cdot 10^{-4}$	2.2	0.40	0.60

The 1D Driftflux model is a transient model, but closure relationships for the particle velocity u_s are based on experimental data of laboratory circulating flow loops and attained under steady-state conditions. On top of this, u_s and c are cross section area averaged values in the 1D model, while in fact a vertical concentration distribution is present in horizontal pipes, caused by settling of the particles. Therefore we ask the question, to what extent is the 1D transient model valid?

In [29] it was found that the steady-state vertical concentration distribution can be estimated using the integrated transient equations of the vertical sediment velocity (in a horizontal pipe). This suggests that these are stable, and any perturbation will lead to a steady-state concentration profile. How quickly this steady-state concentration profile develops was studied in [30] using a numerical analysis. A perturbed concentration profile was found to find its steady state solution within several hydraulic time unit $\frac{h}{u^*}$, with h= height of the profile and u^*= the shear velocity. Concluding, when a concentration profile is subject

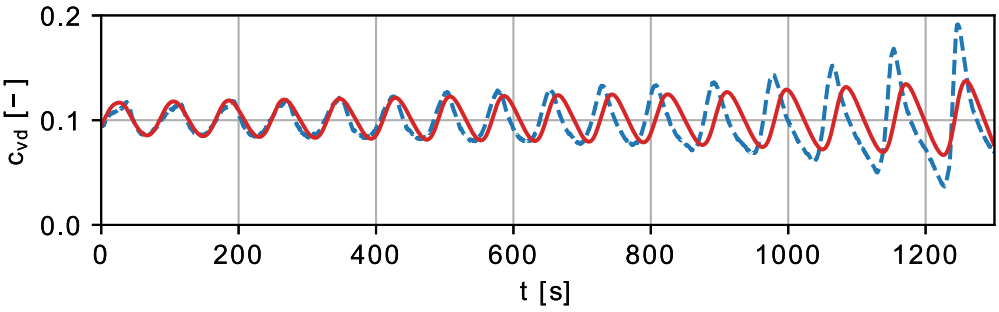

(a) Simulation using $u_{crit} = 2.5\,m/s$ $(+10\%)$

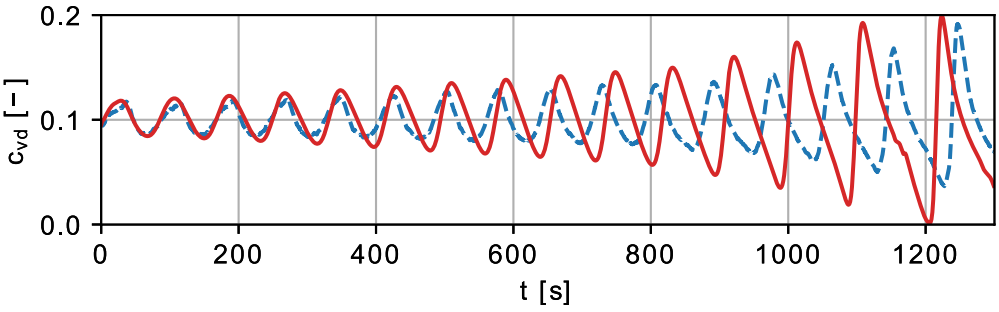

(b) Simulation using $u_{crit} = 2.1\,m/s$ (-10%)

Fig. 14. Sensitivity demonstration of the experiment 1 simulation. Blue: data, red: simulation. Sand, $d_m = 741\,\mu m$, $c = 0.05 - 0.10$.

to changes of c and u_s that occur in a time scale several times larger than the hydraulic time unit, then the concentration profile can be considered as fully developed. Thus we can state that any empirical model of $u_{s/m}$, even when attained in the presence of density waves, is considered a valid model when the conditions as explained above are met. As such, this validity condition also defines the validity of the 1D model. A time scale for a density wave can be estimated from the wave length and the average velocity. For the 1D model to be valid the density wave time scale should far exceed the hydraulic time scale.

$$\frac{L_w}{u_m} >> \frac{D}{u^*} \tag{42}$$

With D= pipe diameter, u^*= shear velocity, L_w= density wave length and u_m= the average mixture velocity. The density waves studied in this research have wave lengths equal to the system length, which was also experienced in [4]. Furthermore, in an open system pipeline the wave lengths are several hundreds of meters [1,3,5]. Considering the long wave lengths of these types of density waves, the validity criterion described by Eq. (42) is easily met and therefore the 1D model can be used to model these types of density waves.

Table 3
The results of the sensitivity analysis of the horizontal relative velocity model. Given are the average values of $u_{s/m}$ in the simulation of experiment 1, as a function of u_{crit}. Values are calculated at $c = 0.1$ and $u_m = 3.5 m/s$.

$u_{crit}[m/s]$	$\frac{u_{crit}}{u_{crit,0}}[-]$	$u_{s/m}[m/s]$	$\frac{u_{s/m}}{u_{s/m,0}}[-]$	Note
2.3	0%	0.93	0%	Reference, used in Fig. 10
2.5	+10%	1.07	+15%	Used in Fig. 14a
2.1	−10%	0.80	−14%	Used in Fig. 14b
2.7	+17%	1.22	+31%	Simulation stopped $c < 0$
1.6	−30%	0.51	−45%	No amplification, but damping

6. Conclusion

The density wave amplification mechanism studied in this article occurs for mixture velocities far above the deposit limit velocity, and can be attributed to the transient accumulation mechanism. Transients accumulation is a complex interaction between spatial particle velocity changes (due to pipe orientation), and global mixture velocity variations due to the changing centrifugal pump load caused by density wave flowing from vertical pipes into horizontal pipes. The proposed 1D Driftflux model accounts for these effects, and is shown to be able to predict density wave amplification to great satisfactory. Since the 1D Driftflux model predicts density wave amplification so well, we consider this as further proof for the existence of a previously unknown density wave amplification mechanism. In addition the model also showed that it predicts fine details, such as the saw-tooth shape of the wave, the wave length and the systems response due to rapid pump revolution changes.

The accuracy of the closure relationships used in the 1D Driftflux model has been explored in this article. Resistance models and the pump related models do not effect the predictive capabilities significantly, however the particle velocity models do. The state of the art in predicting particle velocities in horizontal flows are currently iterative two layer models [25]. The focus of this research was on the development of the 1D model framework, therefore a non-iterative less advanced empirical model was applied. Interesting follow up work would be to implement the two-layer models, to improve the predictive capabilities of the 1D transient model.

Because transient accumulation occurs at mixture velocities far above the deposit limit velocity, the conventional steady-state design method is flawed for designing systems with relatively long vertical pipes combined with horizontal pipes transporting coarse materials, for instance for deep sea mining applications. It is therefore recommended to extend the steady-state design method with a transient

density wave analysis using 1D Driftflux modeling. Future work will aim at understanding which configurations of vertical and horizontal pipelines show amplification, how amplification occurs in open systems and preventive measures to avoid amplification.

CRediT authorship contribution statement

E. de Hoog: Conceptualization, Methodology, Investigation, Validation, Formal analysis, Writing – original draft. **J.M. van Wijk:** Conceptualization, Investigation, Validation, Writing – review & editing. **A.M. Talmon:** Writing – review & editing, Supervision. **C. van Rhee:** Writing – review & editing, Supervision.

Declaration of Competing Interest

The authors declare that they have no known competing financial interests or personal relationships that could have appeared to influence the work reported in this paper.

Acknowledgments

This research is funded by Royal IHC and TKI Maritiem. The Freiberg experiments received funding from the 7th EU Research Framework Programme, grant agreement number 604500. These experiments were conducted by Royal IHC (Kinderdijk, the Netherlands) and the TU Bergakademie Freiberg (Freiberg, Germany).

References

[1] V. Matoušek, Unsteady solids flow in a long slurry pipeline with pumps in series - process of material aggregation, J. Hydrol. Hydromech. 44 (6) (1996) 396–409.
[2] V. Matoušek, Flow Mechanism of Sand-Water Mixtures in Pipelines, Phd thesis Delft University of Technology, Delft, Netherlands, 1997.
[3] A.M. Talmon, Mathematical analysis of the amplification of density variations in long-distance sand transport pipelines, 14th International Conference on Slurry Handling and Pipeline Transport, Maastricht, the Netherlands 1999, pp. 3–20.
[4] A.M. Talmon, L. Aanen, R. Bakker-Vos, Laboratory tests on self-excitation of concentration fluctuations in slurry pipelines, J. Hydraul. Res. 45 (5) (2007) 653–660, https://doi.org/10.1080/00221686.2007.9521801.
[5] E. de Hoog, A.M. Talmon, C. van Rhee, Unstable transients affecting flow assurance during hydraulic transportation of granular two phase slurries, J. Hydraul. Eng. 147 (9) (2021) 1–12, https://doi.org/10.1061/(ASCE)HY.1943-7900.0001913.
[6] T. Mueller, J.M. van Wijk, H. Mischo, Eu blue mining project - building a large scale test system and flow tests for vertical transport systems in deep sea mining, GeoResour. J. 3 (2018) 38–45.
[7] J.M. van Wijk, Vertical Hydraulic Transport for Deep Sea Mining: A Study into Flow Assurance, Phd thesis Delft University of Technology, Delft, Netherlands, 2016. https://doi.org/10.4233/uuid:2e493b95-486a-4c2f-a8ae-749990b06a5e.
[8] K.C. Wilson, G.R. Addie, A. Sellgren, R. Clift, Slurry Transport Using Centrifugal Pumps, 3rd edition Springer, US, 2006.
[9] J.F. Richardson, W.N. Zaki, Sedimentation and fluidisation: Part I, Trans. Inst. Chem. Eng. 32 (1954) 35.
[10] G.V. Messa, S. Malavasi, Numerical prediction of dispersed turbulent liquid–solid flows in vertical pipes, J. Hydraul. Res. 52 (5) (2014) 684–692, https://doi.org/10.1080/00221686.2014.939110.
[11] J. Garside, M.R. Al-Dibouni, Velocity-voidage relationships for fluidization and sedimentation in solid-liquid systems, Indus. Eng. Chem. Process Des. Develop. 16 (2) (1977) 206–214.
[12] R.I. Ferguson, M. Church, A simple universal equation for grain settling velocity, J. Sediment. Res. 74 (6) (2004) 933–937.
[13] J. Sobota, S.I. Kril, Liquid and solid velocity during mixture flow, in: Univ. Paderborn (Ed.), Proc. 19th Int. Kolloquium Massenguttransport durch Rohrleitungen, 1992.
[14] R. Clift, D.H. Manning Clift, Continuous measurement of the density of flowing slurries, Int. J. Multiphase Flow 7 (5) (1981) 555–561, https://doi.org/10.1016/0301-9322(81)90058-6.
[15] M. Ishii, T. Hibiki, Thermo-Fluid Dynamics of Two-Phase Flow, Springer Science, New York, N.Y, 2006.
[16] J. Goeree, Drift-Flux Modeling of Hyper-Concentrated Solid-Liquid Flows in Dredging Applications, Phd, Delft University of Technology, Delft, 2018.
[17] S.L. Soo, On one-dimensional motion of a single component in two phases, Int. J. Multiphase Flow 3 (1) (1976) 79–82, https://doi.org/10.1016/0301-9322(76)90037-9.
[18] B.T. Chao, W.T. Sha, S.L. Soo, On inertial coupling in dynamic equations of components in a mixture, Int. J. Multiphase Flow 4 (2) (1978) 219–223, https://doi.org/10.1016/0301-9322(78)90046-0.
[19] W.C. Verloop, The inertial coupling force, Int. J. Multiphase Flow 21 (5) (1995) 929–933, https://doi.org/10.1016/0301-9322(95)00029-W.
[20] C. Hirsch, Numerical Computation of Internal and External Flows: Fundamentals of Computational Fluid Dynamics / Charles Hirsch, 2nd edition Butterworth-Heinemann, Amsterdam and London, 2007.
[21] R.G. Gillies, C.A. Shook, J. Xu, Modelling heterogeneous slurry flows at high velocities, Can. J. Chem. Eng. 82 (5) (2004) 1060–1065.
[22] D.M. Newitt, J.F. Richardson, M. Abbot, R.B. Turtle, Hydraulic conveying of solids in horizontal pipes, Trans. Inst. Chem. Eng. 33 (1955) 93–113.
[23] E. de Hoog, J.M. in't Veld, J.M. van Wijk, A.M. Talmon, An experimental study into flow assurance of coarse inclined slurries, 18th Conference on the Transport and Sedimentation of solid particles, Prague, Czech Republic 2017, pp. 113–120.
[24] S.A. Miedema, R.C. Ramsdell, Slurry Transport: Fundamentals, A Historical Overview & The Delft Head Loss & Limit Deposit Velocity Framework, 2nd Edition, TU Delft Open Access 2019.
[25] V. Matoušek, J. Krupicka, M. Kesely, A layered model for inclined pipe flow of settling slurry, Powder Technol. 333 (2018) 317–326, https://doi.org/10.1016/j.powtec.2018.04.021.
[26] G.I. Taylor, The dispersion of matter in turbulent flow through a pipe, Proceed. Royal Soc. London Ser. A Math. Phys. Sci. 223 (1155) (1954) 446–468, https://doi.org/10.1098/rspa.1954.0130.
[27] J.M. van Wijk, C. van Rhee, A.M. Talmon, Axial dispersion of suspended sediments in vertical upward pipe flow, Ocean Eng. 92 (2014) 20–30, https://doi.org/10.1016/j.oceaneng.2014.09.041.
[28] A.J. Stepanoff, Pumps and Blowers., Selected Advanced Topics. Two-Phase Flow; Flow and Pumping of Solids in Suspension and Fluid Mixtures, John Wiley & Sons Inc., New York, USA, 1965.
[29] G.H. Keetels, Global Stability of Concentration Profiles in Uniform Sediment-Laden Channel Flow, 18th Conference on the Transport and Sedimentation of Solid Particles, Prague, Czech Republic, 2017.
[30] G.H. Keetels, J.C. Goeree, C. van Rhee, Advection-diffusion sediment models in a two-phase flow perspective, J. Hydraul. Res. 56 (1) (2018) 136–140, https://doi.org/10.1080/00221686.2017.1289262.